# Catalysis Science & Technology



PAPER View Article Online
View Journal | View Issue



**Cite this:** *Catal. Sci. Technol.*, 2022, **12**, 5970

# Single-site, Ni-modified Wells-Dawson-type polyoxometalate for propylene dimerization†

Galiya Magazova, Yoonrae Cho, D Jessica A. Muhlenkamp and Jason C. Hicks D\*

Olefin oligomerization is an essential step in the production of liquid fuels, chemicals, and chemical precursors. Here, we report gas phase propylene oligomerization catalyzed by isolated Ni<sup>2+</sup> sites substituted on the lacunary defect of a Wells–Dawson polyoxometalate ( $K_8P_2W_{17}O_{61}$ ·Ni<sup>2+</sup>) supported on SBA-15 (Ni-POM-WD/SBA-15). The Ni-POM-WD/SBA-15 catalyst exhibited high product selectivity for linear propylene dimers (>76%) relative to branched propylene dimers (<24%). The linear dimer selectivity was independent of the overall propylene conversion between 0.6–5% but was dependent on reaction temperature. The propylene dimerization activation energy was measured as 44.5 kJ mol<sup>-1</sup>, which is consistent with the reported values for Ni<sup>2+</sup> exchanged-zeolites for propylene oligomerization. Further, the measured dimerization reaction rate order was a strong function of the initial propylene partial pressure and transitioned from second order to first order at higher propylene partial pressures. The catalyst was fully regenerated after reaction by applying a thermal regeneration step in helium. Transient, time-on-stream catalyst performance measurements showed the catalyst had a mean life of ~0.6–1.15 h during three reaction cycles and had a slightly increased initial propylene consumption rate with each cycle.

Received 13th June 2022, Accepted 24th August 2022

DOI: 10.1039/d2cy01065h

rsc.li/catalysis

# 1. Introduction

Light alkene oligomerization is an important step to produce a wide range of high-value products for petrochemicals, liquid fuel products, detergents, and lubricants. 1-3 By controlling the catalyst type and structure, linear alpha olefins can be synthesized as valuable precursors for polymers, plasticizers, and surfactants, while internal olefins with linear structure are used in the production of detergents and lubricants.<sup>4,5</sup> The selective dimerization of C3-C8 alpha olefins to linear products has been reported with soluble Fe-, Co-, and Nibased catalysts activated by methylaluminoxane and/or tris(pentafluorophenyl)borane.6-12 However, soluble catalysts have intrinsic limitations due to the difficult phase separation between the metal complex dissolved in organic solvent and products along with the activation step that often requires use of pyrophoric methylaluminoxane co-catalysts. 13,14 Therefore, efforts have been aimed toward developing solid, insoluble catalysts that are easier to recycle, less affected by feed impurities, and active in the absence of co-catalysts.

Nickel-based catalysts have been extensively studied in both academia and industry for olefin oligomerization

Department of Chemical and Biomolecular Engineering, 250 Nieuwland Hall University of Notre Dame, Notre Dame, IN 46556, USA. E-mail: jhicks3@nd.edu † Electronic supplementary information (ESI) available. See DOI: https://doi.org/10.1039/d2cy01065h

reactions due to their high selectivity toward oligomers and high activity without the addition of external activators and co-catalysts for oligomerization reactions. 15-21 Specifically, Ni<sup>2+</sup> cations exchanged on zeolites, such as MFI and FAU, yield liquid propylene oligomerization products at conditions between 180-270 °C and 1-5 bar. 22,23 Ni2+ cations have also been successfully immobilized mesoporous aluminosilicates such as amorphous silica-alumina and Al-MCM-41.3,22,24-27 A common disadvantage of these catalysts is the trade-off between catalytic activity and selectivity to linear products. Moreover, the rate of deactivation and degree of deactivation with time-on-stream have been related to the Ni loading.<sup>27,28</sup> For instance, Mlinar et al. reported that as the Ni site density is increased above 0.6 wt% Ni loading on Na-X zeolite, the maximum turnover frequency decreased and the deactivation order increased.<sup>27</sup> The deactivation was hypothesized as being caused by the formation of inactive, bridged Ni2+-alkyl complexes.27 In addition, the presence of Brønsted acid sites that are needed for the Ni ion exchange can lead to catalyst deactivation via formation of heavier products from the primary alkenes, which can block the pores of the catalyst and poison the active sites.<sup>3,26</sup> The deactivation is hypothesized as being caused by the formation of two neighboring Ni2+-alkyl complexes that are bridged by a common olefin, which are inactive for further C-C coupling.<sup>27</sup> To enhance the production of linear propylene oligomerization products, Ni2+-containing metalorganic frameworks (MOFs) have been explored.<sup>29-31</sup> The

reported Ni2+ cations contained at the nodes of MOFs were 99% selective for oligomers and 95% selective for dimers at 453 K and 5 bar propylene partial pressure.<sup>29</sup> The achieved dimer branching was ~38% at conversions less than 1%, which is superior to the Ni-Na-X catalyst that has comparable activity. Mlinar et al. explained that the improved selectivity towards linear products could be due to increased sterics around the catalyst that favors the formation of linear alkyl intermediates bonded to the Ni<sup>2+</sup> sites, because the Ni<sup>2+</sup> ions are incorporated within the framework of MOF.29 However, MOF containing Ni complexes typically operate at their optimum in condensed phase with activation by organoaluminium compounds at nearly temperature, which limits their applicability. 30-33

Polyoxometalates (POMs) are metal oxide clusters that present unique and well-defined molecular structures that can be formed in a variety of elemental compositions.34-36 POMs have been widely studied for applications in homogeneous and heterogeneous catalysis, because the catalytic properties of POMs can be modulated by changing the central atom, addenda atoms, and/or countercations. 34,35 Supported POMs have been tested for oxidation, dehydration, alkylation, and olefin oligomerization reactions.37-46 Additional anionic charges are created by introducing a vacant site or multiple vacant sites to fully occupied POMs, resulting in lacunary POMs (mono-, di, and trivacant POMs).<sup>47</sup> As-synthesized POMs with lacunary defects can be used as base catalysts for chemical fixation of CO<sub>2</sub>, condensation, dehydration Knovenagel cyanosilylation and biodiesel synthesis. 48-53 The catalytic properties of the existing POMs can be further tuned by transition-metal substitution of the lacunary POM defects. Substitution of Fe, Ag, Mn, Co, Ni, Zn, and Cu into lacunary POMs defects have been reported as redox catalysts.<sup>54–58</sup>

Recently, we observed Ni-substituted Wells-Dawson-type POM (K<sub>8</sub>P<sub>2</sub>W<sub>17</sub>O<sub>61</sub>·Ni<sup>2+</sup>) supported on SBA-15 (Ni-POM-WD/ SBA-15) was active for ethylene oligomerization without added co-catalyst.<sup>59</sup> Ni-POM-WD/SBA-15 achieved an ethylene consumption rate of 152 mmol  $g_{cat}^{-1}$   $h^{-1}$   $(4.22 \times 10^{-5}$  mol  $g_{cat}^{-1}$  s<sup>-1</sup>) at 200 °C and 2 MPa of ethylene partial pressure, which is comparable to reported Ni-based catalysts.<sup>59</sup> For instance, Ni-SiO2-Al2O3 exhibited ethylene oligomerization rates of 0.7-2.7  $\times$  10<sup>-5</sup> mol  $g_{cat}^{-1}$  s<sup>-1</sup> at 170-230 °C and 1.5-3.5 MPa.<sup>60</sup> Ni-BEA showed ethylene oligomerization rates of  $0.6\text{--}1.8 \times 10^{-5} \text{ mol g}_{\text{cat}}^{-1} \text{ s}^{-1} \text{ between 170-270 °C and 0.17-0.4}$ MPa.61 Recently, Seufitelli and Gustafson reported ethylene oligomerization with a Ni-SIRAL catalyst with rates of 11.1  $\times$  $10^{-5}$  mol  ${g_{cat}}^{-1}~s^{-1}$  at supercritical conditions (200 °C and 65 bar).62 The observed ethylene dimers over Ni-POM-WD/SBA-15 were exclusively linear butenes, which was expected for transition metal-catalyzed olefin oligomerization proceeding through the Cossee-Arlman pathway. 13 The measured kinetic parameters were consistent with Ni<sup>2+</sup> exchanged on zeolites, the apparent activation energy was averaged at 41 kJ mol<sup>-1</sup> and reaction rate order was estimated as 1.9. In addition, Ni-POM-WD/SBA-15 was successfully regenerated after ethylene oligomerization reaction *via* helium treatment at 300 °C.<sup>59</sup> Moreover, the dispersion of Ni-POM-WD on the support was shown to be critical, as the unsupported Ni-POM-WD showed no catalytic activity for ethylene oligomerization at 200 °C and 2 MPa due to inaccessibility to Ni sites in the unsupported crystals.<sup>59</sup>

Here, we report the performance of a Ni-substituted Wells–Dawson POM for propylene dimerization. The catalytic performance, regenerability, and the kinetic parameters of Ni sites on Ni-POM-WD/SBA-15 for propylene dimerization were determined and compared to literature reports. We include a detailed analysis of the C6 products formed from propylene oligomerization and compare the selectivity to linear products with Ni-POM-WD to that of a benchmark Ni–K-BEA catalyst. With Ni-POM-WD/SBA-15, we demonstrate selective production of linear dimers from propylene exceeding that of Ni–K-BEA catalyst evaluated at the same condition.

# 2. Experimental

#### 2.1 Catalyst preparation

Ni-POM-WD/SBA-15 was synthesized by following reported procedures.<sup>57–59,63,64</sup> First, 100 g of Na<sub>2</sub>WO<sub>4</sub>·2H<sub>2</sub>O (Alfa Aesar, 99.0-101.0%) was added to 350 mL of deionized water (18.2  $M\Omega$ ), heated to reflux, and stirred under reflux until fully dissolved. Then, phosphoric acid (Millipore Sigma, 85%) was slowly added dropwise to the refluxing solution and stirred under reflux for 24 h. After the solution was cooled to room temperature, 100 g of potassium chloride (BDH Chemicals, 99.0-100.5%) was added to precipitate the crude mixture. The isomeric mixture of α/β-K<sub>6</sub>P<sub>2</sub>W<sub>18</sub>O<sub>62</sub> was obtained after recrystallization of the crude precipitate. The mixture of  $\alpha/\beta$ - $K_6P_2W_{18}O_{62}$  was purified to  $\alpha$ - $K_6P_2W_{18}O_{62}$  by sequential pHcontrolled base degradation and re-acidification steps. Lacunary POM-WD (K<sub>10</sub>P<sub>2</sub>W<sub>17</sub>O<sub>61</sub>) was prepared by adding 1 M KHCO<sub>3</sub> to an aqueous solution of α-K<sub>6</sub>P<sub>2</sub>W<sub>18</sub>O<sub>62</sub>, and the formed crystals were collected after recrystallization via filtration. Ni-POM-WD  $(K_8P_2W_{17}O_{61}Ni^{2+})$  was synthesized by mixing a stoichiometric amount of Ni(NO<sub>3</sub>)<sub>2</sub>·6H<sub>2</sub>O (Alfa Aesar, 98%) and lacunary POM-WD in water. The precipitate was isolated by filtration. Each synthesis was confirmed by a solution 31P NMR to analyze the phosphorous features. The  $^{31}P$  NMR peaks for  $\alpha/\beta$ -K<sub>6</sub>P<sub>2</sub>W<sub>18</sub>O<sub>62</sub> POM mixture, α-POM-WD (α-K<sub>6</sub>P<sub>2</sub>W<sub>18</sub>O<sub>62</sub>), lacunary POM-WD  $(K_{10}P_2W_{17}O_{61})$  and Ni-POM-WD  $(K_8P_2W_{17}O_{61}\cdot Ni^{2+})$  are shown in Fig. S1.† After the purification the α/β-K<sub>6</sub>P<sub>2</sub>W<sub>18</sub>O<sub>62</sub> POM mixture, one phosphorous peak was observed at -13.1 ppm, which is associated with internal phosphates of α-POM-WD (Fig. S1a and b†). Introducing a vacant site to create lacunary POM-WD resulted in a new phosphorus peak at -7.5 ppm, due to a changed environment around the phosphate closest to the vacant site (Fig. S1c†). Introducing nickel to the defect site of the lacunary POM-WD resulted in a shift of the peak at -7.5 ppm to 200-250 ppm region, due to the paramagnetic effect caused by Ni2+ (Fig. S1d†). 31P NMR peaks at these locations correspond to successful metalation of the lacunary POM-WD

by Ni. 57-59,63 From our previous studies, single crystal XRD of Ni-POM-WD crystals indicates that the Ni sites substitute one of the three tungsten atoms in capping regions of a WD POM, eliminating the probability of the Ni sites being outside of the defect position.<sup>59</sup> In addition, Ni loading of unsupported Ni-POM-WD obtained by ICP corresponds to the nominal loading.59

SBA-15 was prepared using the synthesis procedures described elsewhere. 65,66 First, 18 g of Pluronic 123 (Sigma-Aldrich) and 99.5 g of hydrochloric acid (Millipore Sigma, 37%) were fully dissolved in 550 g of deionized water. Then, to the prepared mixture, 39.8 g of tetraethyl orthosilicate (Acros Organics, 98%) was added, and the solution was held at 35 °C for 20 h and 80 °C for 24 h. The formed solid was collected by vacuum filtration and washed with ~1 L of deionized water, then dried overnight at 60 °C. The material was calcined in air at 200 °C at a ramp rate of 1.2 °C min<sup>-1</sup> for 1 h, then at 550 °C at a ramp rate of 1.2 °C min<sup>-1</sup> for 6 h. Finally, SBA-15 was vacuum dried at 200 °C for 3 h and stored under N2 in a glove box.

Ni-POM-WD/SBA-15 was prepared by first dissolving 0.161 g of Ni-POM-WD in deionized water to synthesize ~1.5 g 10 wt% Ni-POM-WD/SBA-15. The dissolved Ni-POM-WD was impregnated on SBA-15 with a ratio of 1.6 mL solution per gram of solid via incipient wetness and subsequently dried under air at 100 °C. 59,66 The Ni-POM-WD/SBA with 1 wt% Ni-POM-WD was synthesized similarly to 10 wt% Ni-POM-WD/ SBA by using 0.0161 g of Ni-POM-WD. Ni-POM-WD on fumed silica was synthesized on a commercial fumed silica (Sigma-Aldrich), following the same procedure as for Ni-POM-WD/ SBA synthesis, and the resulting material contained 10 wt% Ni-POM-WD.

Ni-K-BEA was synthesized by following reported procedures.<sup>25</sup> Ni-K-BEA was synthesized starting from commercial NH<sub>4</sub>-BEA (Alfa Aesar, SiO<sub>2</sub>: Al<sub>2</sub>O<sub>3</sub> = 38:1). NH<sub>4</sub>-BEA was first calcined in air at 500 °C for 4 h to form H-BEA. Then H-BEA was ion exchanged with potassium at room temperature for 24 h using 1 M aqueous KNO<sub>3</sub> (Alfa Aesar, 99%) with a ratio of 100 mL of solution per gram of solid. The pH of the solution was controlled to maintain pH ~7 using 0.1 M KOH (BDH, 85%) solution. K-BEA was collected by centrifugation, washed with deionized water, dried at 80 °C overnight, and calcined in air at 500 °C for 4 h. K-BEA was further exchanged with nickel and potassium at room temperature for 24 h using an aqueous solution of 0.04 M Ni(NO<sub>3</sub>)<sub>2</sub> (Alfa Aesar, 98%) and 1 M KNO<sub>3</sub> with a ratio of 100 mL of solution per a gram of solid. The pH of the solution was controlled to maintain pH ~7 using 0.1 M KOH solution. The final material Ni-K-BEA was collected by centrifugation, washed with water, dried at 80 °C overnight, and calcined in air at 500 °C for 4 h.

#### 2.2 Catalyst characterization

Solid-state <sup>31</sup>P NMR was performed on Ni-POM-WD/SBA-15 as prepared and after the reaction was performed using a JEOL ECX-300 at a spin rate of 10 kHz. The samples were packed in 3.2 mm zirconia sample rotors.

Solution 31P NMR on Wells-Dawson polyoxometalate and its derivatives was performed by a Bruker AVANCE III HD 400 MHz Nanobay. Samples were dissolved in a mixture of 90% water and 10% D<sub>2</sub>O prior to the analysis.

Elemental analysis on Ni-POM-WD/SBA-15 and Ni-K-BEA was performed via inductively coupled plasma-optical emission spectroscopy (ICP-OES) using a Perkin Elmer Optima 8000. The materials were added to 0.8 M of KOH solution at room temperature with a ratio of 10 mg of sample per 10 g of base until the silica was fully dissolved. Then, 5 g of the mixture was dissolved in 75 g of a 2 vol% HNO<sub>3</sub> aqueous solution. Si, Al, and Ni contents were quantified using external calibration curves, which were prepared with silicon (BDH, 1000 μg mL<sup>-1</sup> in 1% HNO<sub>3</sub> matrix), aluminum (RICCA, 1000 µg mL<sup>-1</sup> in 3% HNO<sub>3</sub> matrix), and nickel (BDH, 100 μg mL<sup>-1</sup> in 2% HNO<sub>3</sub> matrix) standards.

High-angle annular dark-field scanning transmission electron microscopy (HAADF-STEM) and energy dispersive X-ray spectroscopy (EDX) on Ni-POM-WD/SBA-15 were conducted using a spectra 30-300 transmission electron microscope. Samples were prepared by dispersing in acetone using sonication and then drop casting onto a carbon coated copper grid.

#### 2.3 Propylene oligomerization reactions

Propylene oligomerization experiments were performed in a stainless steel, fixed-bed reactor (i.d. = 6.35 mm) in the ranges of 80-180 °C and 1-6 bar. Helium (Airgas, ultra high purity) and propylene (Airgas, polymer grade) were purified by in-line moisture traps (Matheson). For each reaction, 200 mg of catalyst was pelletized, sieved (150-250 µm) and diluted in 300 mg of Davisil® silica (150-250 µm). Prior to reaction testing, the catalyst was pre-treated under pure helium at 300 °C for 12 h to free the catalyst from moisture, and then the reactor was cooled to the reaction temperature. For the pressure sweep experiments, the reactor was pressurized to 1-6 bar by a back-pressure regulator (Sweagelok). The reactor outlet was directly connected to an SRI 8610C GC-FID equipped with MXT-Wax

15 m (Restek) and MXT-Alumina BOND/MAPD 30 m (Restek) columns for product analysis. External standards were separately injected to identify all products formed: 1-hexene (Sigma-Aldrich, ≥99%), trans-2-hexene (Acros Organics, >98%), cis-2-hexene (Alfa-Aesar, 96%), trans-3hexene (TCI,  $\geq$ 99%), cis-3-hexene (TCI,  $\geq$ 97%), 2-methyl-2pentene (TCI, ≥95%), 2-methyl-1-pentene (Acros Organics, 99%), 4-methyl-1-pentene (Thermo Scientific, ≥98%), trans-4methyl-2-pentene (TCI, ≥97%), 3-methyl-1-pentene (TCI, >98%), trans-3-methyl-2-pentene (TCI, >99%), cis-3-methyl-2pentene (TCI, ≥95%), 2,3-dimethyl-1-butene (TCI, ≥98%) were used for product identification.

The propylene conversion, propylene consumption rate, and product selectivity were calculated according to eqn (1)-

(3), respectively. 67,68 The carbon mass balance was >99% for all reaction runs.

Propylene conversion (%)

$$= \frac{\text{moles of carbon detected in the overall products}}{\text{overall moles of carbon detected at the outlet}} \times 100$$

(1)

(2)

Propylene consumption rate (h<sup>-1</sup>)

propylene inlet flowrate (mol h-1) × propylene conversion

mol Ni in POM or zeolite loaded into reactor

Product selectivity (%)

(3)

moles of carbon in a specific product moles of carbon in all detected products

# 3. Results and discussion

#### 3.1 Catalyst characterization

We begin by providing structural characterization of the synthesized Ni-substituted Wells-Dawson catalyst and the control materials. The textural properties, as well as the elemental analysis of Ni-POM-WD/SBA-15, SBA-15, H-BEA and Ni-K-BEA are presented in Table 1. As expected, the BET surface area and BJH pore volume of the initial SBA-15 decreased upon impregnation of 1 wt% and 10 wt% Ni-POM-WD (Fig. S2†). The micropore volume of Ni-K-BEA is consistent with previously published Ni2+ exchanged on beta zeolites (Fig. S3†).69 The solid-state MAS 31P NMR indicates that the Ni-POM-WD structure remains unaltered after impregnation on SBA-15, and it is in agreement with the reported literature (Fig. S5a†).<sup>59</sup> A peak at -21.6 ppm represents a phosphate away from the substituted Ni site.

HAADF-STEM image of as-synthesized Ni-POM-WD/SBA-15 with 10 wt% Ni-POM-WD is given in Fig. 1a. Fig. 1 shows the particles ascribed to Ni-POM-WD clusters and depicts that the POM structures are highly dispersed across the SBA-15 pore structure. Fig. 1b shows that after Ni-POM-WD impregnation SBA-15 retains the clear pattern with parallel stripes, which corresponds to the unidirectional pore structure of the support. Ni EDX elemental mapping is given in Fig. 1b. Elemental maps of P, K, W, O, and Si are given in Fig. S6.† The EDX mapping shows that not only the POM, but also the Ni, is dispersed evenly throughout the SBA-15 support. This shows that the high surface area of SBA-15 allows for high dispersion of Ni-POM-WD, and therefore increasing accessibility to the Ni sites.

#### 3.2 Product distribution of the dimers

We evaluated the propylene oligomerization performance of Ni-POM-WD/SBA-15 at 180 °C and 1-6 bar total pressure. Fig. 2a shows the product distribution of propylene dimers at various initial conversions. Propylene oligomerization on Ni-POM-WD/SBA-15 resulted in the formation of propylene dimeric products only (C6 species). A temperature programmed desorption experiment on the spent catalyst (ramped from room temperature to 300 °C under helium at a 10 °C min<sup>-1</sup>) using in-line mass spectrometry also yielded C6 olefin products (m/z = 84) with no observation of C9 products. The most prevalent product is trans-2-hexene, followed by trans-3-hexene (Fig. 2a). The other products formed in significant quantities are trans-4-methyl-2-pentene and cis-2-hexene, cis-3-hexene, 4-methyl-1-pentene, and 1-hexene (Fig. 2a). This product distribution remained fairly stable as the initial conversion was varied from 0.6-5%.

The product distribution of the propylene dimers generated on Ni-POM-WD/SBA-15 can be explained by considering the propylene oligomerization mechanism. Longer alkenes generated from propylene over transition metal catalysts follow a propagation step that involves four distinct intermediate stages that depend on insertion of propylene on the metal-hydride and the subsequent metal-alkyl bond.<sup>13</sup> The simplified reaction pathways for propylene oligomerization are illustrated in Scheme 1, which are inspired by the proposed mechanism propylene oligomerization by homogeneous catalysts. 13,70 The catalytic propylene oligomerization starts with the coordination and subsequent insertion of molecules on Ni-H species, which are propylene commonly accepted as active sites, through terminal (1') or internal (2') carbon coupling to Ni-H.25,71 Linear hexenes can only be formed if the first propylene bonds to the nickel ion through 1' (1'-Ni), whereas 2' bonding to a nickel site (2'-Ni) promotes the formation of the monoand di-branched hexenes. Then, the formed Ni-alkyl complexes can react with the second propylene also by either binding to the 1' or 2' carbon, which results in four different intermediates 1'-1', 1'-2', 2'-1' and 2'-2'. The termination step on these different pathways occurs

Table 1 Elemental analysis and nitrogen physisorption pore properties of Ni-POM-WD/SBA-15, SBA-15, H-BEA and Ni-K-BEA

|                           | Elemental analysis |       |                         |                          | BJH pore          | Micropore                        |
|---------------------------|--------------------|-------|-------------------------|--------------------------|-------------------|----------------------------------|
| Sample                    | Ni (wt%)           | Ni/Al | BET area $(m^2 g^{-1})$ | BJH pore<br>diameter (Å) | $ (cm^3 g^{-1}) $ | volume<br>(cm³ g <sup>-1</sup> ) |
| SBA-15                    | _                  | _     | 880                     | 67                       | 0.70              | _                                |
| Ni-POM-WD (10 wt%)/SBA-15 | 0.12               | _     | 560                     | 67                       | 0.50              | _                                |
| Ni-POM-WD (1 wt%)/SBA-15  | 0.011              | _     | 660                     | 67                       | 0.57              | _                                |
| H-BEA                     | _                  | _     | 536                     | 32                       | _                 | 0.22                             |
| Ni–K-BEA                  | 0.84               | 0.27  | 561                     | 32                       | _                 | 0.23                             |

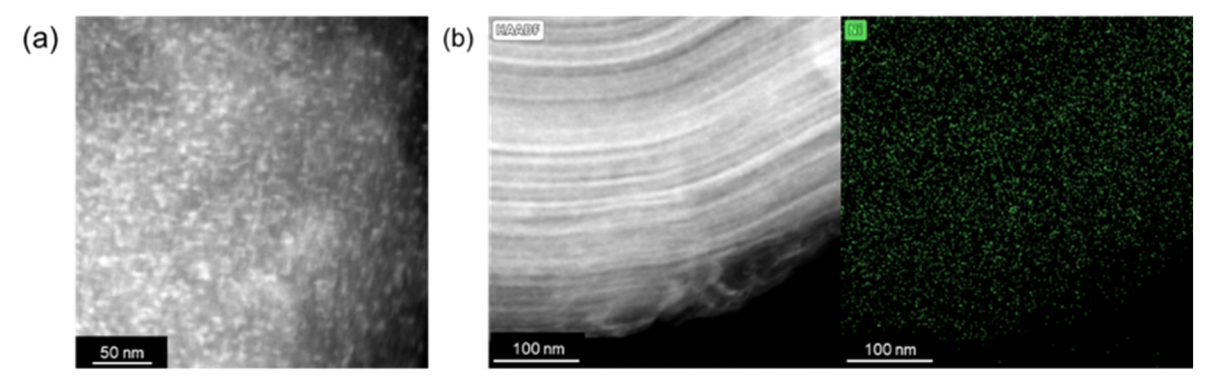


Fig. 1 (a) HAADF-STEM image and (b) EDX Ni mapping of Ni-POM-WD/SBA-15.

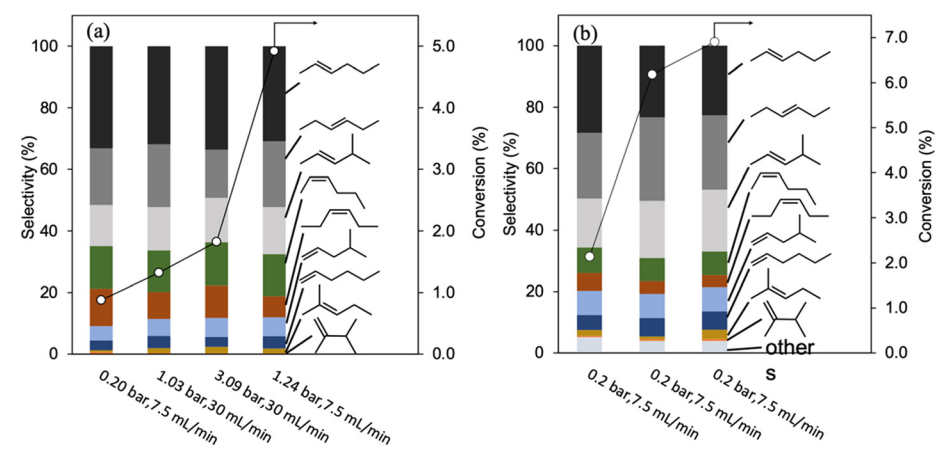


Fig. 2 (a) Propylene oligomerization product selectivity at initial conversions at 180 °C for Ni-POM-WD/SBA-15 (propylene molar rate of 0.02-1.1 mol g<sup>-1</sup> h<sup>-1</sup>) and (b) Ni-K-BEA (propylene space velocities of 0.3-1.7 mol g<sup>-1</sup> h<sup>-1</sup>) (b). The other products of Ni-K-BEA represent non-dimeric products.

Ni-H + 
$$\frac{2'}{2'-Ni}$$
  $\frac{2'}{2'-1'}$   $\frac{1'\cdot 1'}{Ni}$   $\frac{\beta \cdot H}{Ni}$   $\frac{\beta \cdot H}{\beta \cdot H}$   $\frac{isomerization}{cis+trans}$   $\frac{isomerization}{cis+trans}$   $\frac{\beta \cdot H}{\beta \cdot H}$   $\frac{isomerization}{cis+trans}$ 

Scheme 1 Reaction pathways of propylene dimerization to yield primary dimer products in the presence of Ni-based catalysts. The figure was inspired by Mlinar et al.22

through β-hydride elimination and results in 1- and cis/ trans-2-hexene (1'-1'), 2-methyl-1-pentene (1'-2'), 4-methyl-1pentene and 4-methyl-2-pentene (2'-1'), and 2,3-dimethyl-1butene (2'-2'). Moreover, a fast rearrangement of the formed hexenes is possible before the desorption of the products, which leads to secondary products, which cis/trans-3-methyl-pentene, include cis/trans-3-hexene, 2-methyl-2-pentene, and 2,3-dimethyl-2-butene.<sup>72</sup>

High selectivity towards trans-2-hexene, trans-3-hexene, trans-4-methyl-2-pentene, cis-2-hexene, cis-3-hexene, 4-methyl-1-pentene, 1-hexene, and 2-methyl-2-pentene over Ni-POM-WD/SBA-15 suggests that the preferred pathway is adsorption of the second propylene molecule with its terminal carbon (1') on 1'-Ni and 2'-Ni sites, which correspond to intermediates 1'-1' and 2'-1'. Whereas minimal production of 2,3-dimethyl-1-butene (<1%) and lack of 2,3-dimethyl-2-

butene and 2-methyl-1-pentene show that the formation of 2'-2' and 1'-2' is less likely. In addition, cis-4-methyl-2pentene and 2,3-dimethyl-2-butene were not observed at this range of conversions, possibly due to the low rate of isomerization. The lack of cis-4-methyl-2-pentene and 2,3-dimethyl-2-butene propylene dimers was also reported on Ni(II)-MOFs, Ni<sub>2</sub>(dodbc) and Ni<sub>2</sub>(dododc), at similar reaction conditions, 180 °C and 5 bar, and below 2% propylene conversion.<sup>29</sup> Moreover, Fig. 3 shows the selectivity to linear dimers is ~76-80% across the range of initial conversion tested for Ni-POM-WD/SBA-15. The product distribution and the selectivity to linear hexenes after 300 min of time-on-stream (TOS) remained unchanged (Fig. S8a and S9†). A high selectivity to linear products is possible if the initial propylene and additional propylene bind with their terminal carbons on the catalyst sites, and the subsequent hexene skeletal isomerization is limited. 13 Enhanced selectivity for the linear products over solid catalysts has been reported by Mlinar et al. on Ni-modified metal organic frameworks, due to increased steric control of the Ni<sup>2+</sup> sites in the MOF structure.29 Liu and Smit computationally interrogated MOFs and zeolites with different structures to show the relation between product distribution and pore size and reported that the production of linear isomers directly correlated to the free energies of adsorption of linear and branched isomers.<sup>73</sup> The enthalpies and entropies of each product that constitute their free energies strongly depend on the pore size of the catalyst, especially with pore sizes of ~10 Å and lower. The selectivity to linear alkenes increases with the pore size approaching the size of the linear hexenes, whereas the selectivity to branched products is lowered due to steric hindrance.<sup>73</sup>

The average pore size of mesoporous SBA-15 impregnated with 10 wt% Ni-POM-WD is  $\sim$ 68 Å; however, the product distribution is predominantly linear, which implies that the effect of the pore size is negligible. The Ni-POM-WD has a unit cell length of  $\sim$ 20 Å<sup>59</sup> to potentially create confinement effects that favor the formation of linear hexenes. Ni-POM-WD was impregnated with the same loading on fumed silica

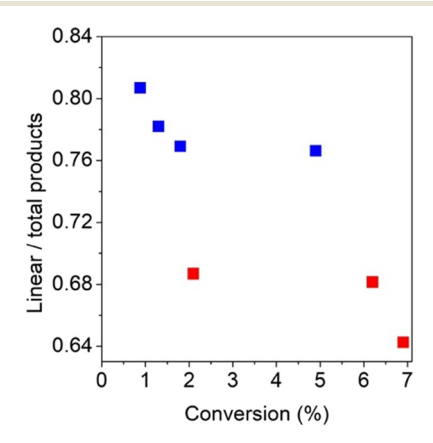
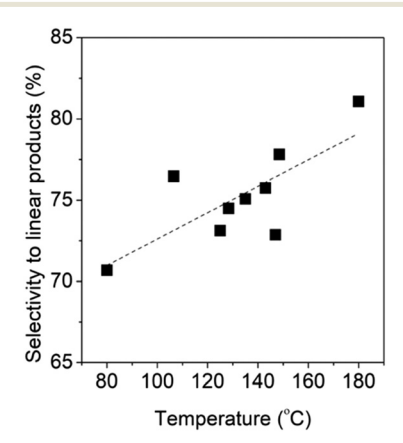


Fig. 3 Selectivity to linear products at initial conversions at 180  $^{\circ}$ C for Ni-POM-WD/SBA-15 (blue) and Ni-K-BEA (red).

(10 wt%), which is a silica support with low porosity (the surface area is 354 m<sup>2</sup> g<sup>-1</sup> and the total pore volume is 0.69 cm3 g-1), to evaluate the degree of linearity of the formed products. The initial selectivity as a function of initial conversion for Ni-POM-WD/fumed silica and Ni-POM-WD/ SBA-15 materials is given in Fig. S10a.† Both catalysts were tested at identical reaction conditions, 180 °C, 1-6 bar total pressure, and propylene molar rate of  $0.02-1.1 \text{ mol g}^{-1} \text{ h}^{-1}$ . The catalytic activity of Ni<sup>2+</sup> sites on fumed silica was significantly lower than the performance of Ni<sup>2+</sup> sites on SBA-15, which implies that SBA-15 improves the dispersion of the Ni-POM-WD. In addition, at similar conversions ( $\sim$ 1%), Ni-POM-WD/fumed silica had ~5% fewer linear products formed than Ni-POM-WD/SBA-15 (Fig. S10b†), implying that Ni-POM-WD within the SBA-15 pore structure may exhibit an enhanced confinement effect that promotes selectivity for linear products.

Moreover, the product selectivity to linear products on Ni-POM-WD/SBA-15 at steady-state, which is an average of the selectivity after 300 min time-on-stream, changes with temperature. As the temperature is increased between 80-180 °C, the selectivity to linear products increases (Fig. 4). The product selectivity remained exclusive toward propylene dimers; trimers and heavier alkenes were not detected with increased temperature. The possible increase in selectivity for linear hexenes with the increased temperature could be due to stronger adsorption of the branched hexenes on the catalyst surface compared to the linear alkenes. With zeolite supported Ni<sup>2+</sup> for butene dimerization, Ehrmaier et al. reported 2-butene on the catalyst surface caused a higher rate of formation of mono- and di-branched species, resulting in faster catalyst deactivation from these strongly adsorbed species on the active sites.<sup>74</sup>

For comparison, a benchmark catalyst, Ni-exchanged on beta zeolites with potassium poisoned Brønsted acid sites (Ni-K-BEA), was tested at similar reaction conditions and conversions to assess the degree of branching (Fig. 2b). Ni-BEA catalyst has been widely reported for ethylene



**Fig. 4** Selectivity to linear products at temperatures between 80–180 °C and 1.01 bar for Ni-POM-WD/SBA-15. The linear fit is shown for guidance.

oligomerization, with multiple reports involving analysis of the observed deactivation behavior. 28,75 The selectivity for dimerization products is ~95% with Ni-K-BEA, while the remaining products are trimers and alkenes with odd carbon numbers. The selectivity to the linear products is  $\sim$ 64-68% at the initial conversions, which is lower than that of Ni-POM-WD/SBA-15 catalyst. The main products with Ni-K-BEA are trans-3-hexene, trans-2-hexene, and trans-4-methyl-2pentene. A larger percentage of secondary isomers indicates that double-bond isomerization or readsorption and isomerization occur more readily on Ni-K-BEA.72 The remaining products are 4-methyl-1-pentene, cis-2-hexene, 1-hexene, 2-methyl-2-pentene, and 2,3-dimethyl-1-butene. However, the linear product selectivity of Ni-K-BEA after 300 min of TOS is ~77%, which is similar to Ni-POM-WD/SBA-15 (Fig. S9†). The residual Brønsted acid sites untitrated by potassium may contribute to the propylene oligomerization reaction along with the Ni<sup>2+</sup> sites at the onset of the reaction and cause a greater degree of branching in the hexene products. After Brønsted acid sites are poisoned by the adsorbed heavier oligomers at longer TOS, Ni<sup>2+</sup> sites likely dominate the observed activity, and the product distribution becomes similar to those exhibited by Ni<sup>2+</sup> in Ni-POM-WD/ SBA-15.

#### 3.3 Measurement of kinetic parameters of Ni-POM-WD

Kinetic evaluation of the catalyst was performed in a flow reactor in the differential regime where propylene conversions were less than 2%. The differential regime of the reactor was verified by space velocity sweep experiments (Fig. S11†). At 180 °C, 1.01 bar, and propylene conversion less than 2%, the propylene consumption rate remained stable with various catalyst contact times. To evaluate the kinetic parameters of the catalyst, the temperature and pressure dependence of Ni-POM-WD/SBA-15 (10 wt% Ni-POM-WD) propylene oligomerization were determined by the average rates at steady-state. Propylene consumption rate was measured between 80-180 °C and 1.01 bar total pressure and plotted as the Arrhenius plot (Fig. 5a). The slope of the fitted

line corresponds to the apparent activation energy and was measured as 44.5 kJ mol<sup>-1</sup>, which is in agreement with the reported values in the literature. 22,27 Fig. 5b and c show the propylene dimerization rate dependence on propylene partial pressure at 180 °C and two different total pressures, 4.5 and 6.2 bar, respectively. The hexenes production rate and propylene pressure have a linear correlation at both 4.5 and 6.2 bar, and the slopes of the linear fits correspond to the reaction rate order (Table S2†). The slope in Fig. 5b shows second order dependence for the dimer formation on propylene partial pressure in the lower pressure regime (4.5 bar), while first order dependence is observed in the higher propylene partial pressure region (6.2 bar) (Fig. 5c). The second order dependence indicates Ni active sites are in abundance and being unsaturated with olefins in the chosen pressure regime. As the partial pressure of the olefin is increased, the Ni sites are occupied by more adsorbed surface species which results in the first order dependency on propylene partial pressure (Table S2†). 60,76,77 Cho et al. reported similar reaction rate order dependency on ethylene partial pressure for butene production while investigating ethylene oligomerization. With a 1 wt% Ni-POM-WD loading on SBA-15 at 0.62 MPa, the authors found the butene production reaction rate followed a second order dependence, whereas at 2 MPa the observed reaction rate followed a first order dependence.<sup>59</sup> The internal and external mass transfer calculations were performed for the rates between 80-180 °C (see section 5 of the ESI†).

# 3.4 Stability of Ni-POM-WD

As-prepared SBA-15, α-POM-WD/SBA-15 and lacunary POM-WD/SBA-15 with no Ni<sup>2+</sup> sites and Ni-POM-WD/SBA-15 (10 wt% Ni-POM-WD) were tested at identical reaction conditions, at 180 °C and 1.01 bar, and the initial propylene consumption rate for each of the materials is given in Fig. 6a. SBA-15, α-POM-WD/SBA-15 and lacunary POM-WD/ SBA-15 showed negligible background activity, which suggests that the observed activity on Ni-POM-WD/SBA-15 emerges from Ni<sup>2+</sup> sites. The small, but observed, propylene

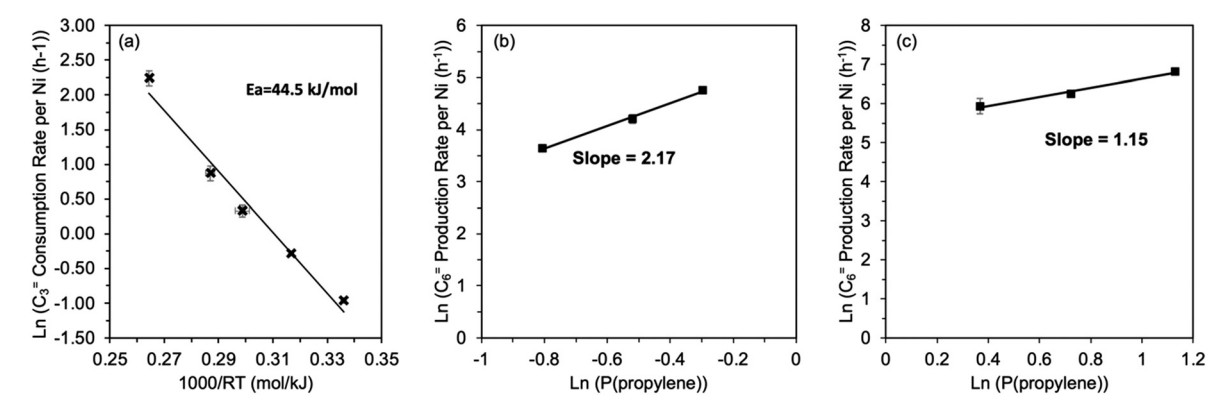


Fig. 5 (a) Arrhenius plot for determination of activation energy between 80-180 °C and 1.01 bar and (b) effect of propylene partial pressure on formation of dimers at 180 °C, 4.5 and (c) 6.2 bar.

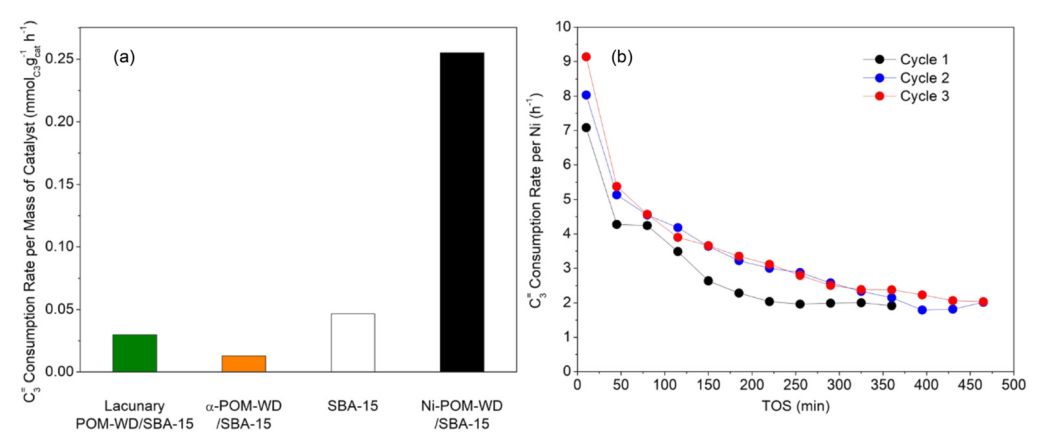


Fig. 6 (a) Initial propylene consumption rate over Ni-POM-WD/SBA-15 and benchmark materials and (b) normalized rate of propylene consumption of recycled catalyst at 180 °C and 1.01 bar.

conversion on the benchmark materials is due to thermal propylene oligomerization under this set of reaction conditions.<sup>78-80</sup> The transient behavior of the catalyst was studied using time-on-stream experiments. The Ni-POM-WD/ SBA-15 was tested at 180 °C and 1.01 bar, and the propylene consumption rate is given in Fig. 6b. According to Fig. 6b, the catalyst undergoes deactivation with time. The fitted deactivation trajectory shows a decay, which can be fitted to the exponential (eqn (S1)†) and hyperbolic (eqn (S2)†) profiles given in Fig. S12.† The deactivation trajectory fitted to the exponential decay indicates a first-order deactivation, which involves a single site being responsible for one deactivation event. The second order deactivation profile (hyperbolic deactivation) involves multiple sites participating in a single deactivation event. 25,27,28,75 Mlinar et al. proposed a deactivation mechanism for Ni-Na-X during propylene oligomerization, which is attributed to Ni<sup>2+</sup> sites migrating during the activation period and subsequently forming Ni dimers with a shared olefin, causing the second order deactivation behavior.<sup>27</sup> Saxena et al. showed that varying the Ni site density in Ni-Li-beta catalyst effected the deactivation order, under identical reaction conditions a catalyst with low Ni site density deactivated following the first order model, and the high Ni density material showed second order deactivation.<sup>28</sup> The first order deactivation was caused by heavier alkene oligomers poisoning Ni sites, whereas the presence of the high Ni site density was hypothesized to result in the formation of bridged alkyl species between two Ni sites. 25,27,28,75

The early TOS (<6 h) data (Fig. S12†) follows both deactivation models, which is consistent with reported attempts to fit the short range of TOS described in the literature.28 Therefore, Ni-POM-WD/SBA-15 was examined with longer TOS (>55 h) as shown in Fig. S13.† The propylene dimers production rate normalized by the total amount of Ni sites was fitted to the first and second deactivation models, as well as to the Butt-Peterson deactivation model<sup>28,75,81</sup> (Fig. S13a†). The Butt-Peterson deactivation model predicts the initial rate, deactivation constant, and the deactivation order as independent parameters, and the model was used in literature to report the deactivation order on Ni-beta, Ni-MCM-41, Ni-FAU-6 and Ni-FAU-40 during oligomerization reactions. 28,75,81 All deactivation equations were modified by adding a steady-state rate constant, because the Ni sites in Ni-POM-WD/SBA-15 did not reach full deactivation, which is different than zeolite-based catalysts. Even after >55 h of TOS, the propylene conversion remained above the thermal background conversion, indicating some of the sites remain active for the Ni-POM-WD/SBA-15 catalyst (Fig. S13b†) while other catalysts completely deactivate. The best fit parameters for all deactivation models are given in Table S3.† All three models have reasonable R2 values; however, the second order deactivation and Butt-Peterson models, which predicts the deactivation order as 2.03, have slightly greater R2 values and smaller normalized absolute errors than those of the first order deactivation model. It should be noted that the number of data points collected at the onset of the reaction could impact the  $R^2$  values. Because the second order deactivation model fits the deactivation profile of Ni-POM-WD/SBA-15 stronger, it is possible that the catalyst follows the second order deactivation. Despite having a low Ni loading (0.12 wt% Ni), the second order deactivation implies that two neighboring Ni sites are participating in a single deactivation event by forming a shared alkyl species. We hypothesize that this is possible due to the mobility of solvated Ni-POM-WD clusters during propylene oligomerization. The synthesized POMs are physically immobilized on the SBA-15 support, which are subject to solvation effects from formed hexenes potentially driving Ni sites to close proximity with each other. To test this hypothesis, a 1 wt% Ni-POM-WD/SBA-15 material with a lower Ni loading (0.011 wt% Ni) was impregnated on SBA-15 and tested at the identical reaction conditions (180 °C and 1.01 bar for  $\sim$ 50 h TOS; Fig. S14a and b†). Similar to the 10 wt% Ni-POM-WD/SBA-15 catalyst, the 1 wt% Ni-POM-WD/ SBA-15 material deactivated with increasing TOS without reaching a complete deactivation. The deactivation trajectory of the propylene dimer production rate per Ni was fitted to

the first order, second order and Butt-Peterson deactivation models as shown in Fig. S14a.† The second order deactivation model and Butt-Peterson model with a 2.3 deactivation order have slightly greater  $R^2$  values and lower normalized absolute error compared to the first order deactivation profile (Table S4†). These results possibly confirm the hypothesis that solvation effects of physisorbed Ni-POM-WD can result in second order site deactivation. Moreover, the catalyst with 1 wt% Ni-POM-WD loading had a slower deactivation rate and a smaller deactivation constant (k<sub>d</sub>) than 10 wt% Ni-POM-WD on SBA-15, where the  $k_{\rm d}$  of 1 wt% and 10 wt% Ni-POM-WD were 0.146 h<sup>-1</sup> and 0.268 h<sup>-1</sup>, respectively. The propylene conversion with 10 wt% Ni-POM-WD material started to reach its steady-state value at ~30 h TOS, while plateauing for 1 wt% Ni-POM-WD began at ~40 h. Lastly, we tested the benchmark Ni-K-BEA catalyst at long TOS and fitted the deactivation profile to compare it to the reported deactivation order for the Ni-beta catalyst. As shown in Fig. S15 and Table S5,† the Ni-K-BEA catalyst has a deactivation profile that is fitted better with the second order deactivation. The catalyst had 0.8 wt% Ni loading and Ni/Al = 0.27, which is similar to Ni-beta catalyst (Ni/Al = 0.25) reported by Saxena et al. 28 They stated that the catalyst with Ni/Al = 0.25 follows the second order deactivation profile during ethylene oligomerization due to high Ni density. Since the benchmark catalyst has a similar Ni/Al ratio, it will likely have the same deactivation behavior as well.

In order to further understand the deactivation of this material, the spent Ni-POM-WD/SBA-15 was regenerated following a procedure described by Cho et al.59 First, the reactor was purged at 180 °C under helium to remove existing products and propylene, then the temperature was increased to 300 °C under helium and held for 12 h to desorb the adsorbed heavy alkenes. The initial activity was fully recovered using this regeneration method, as shown in Fig. 6b and Table 2. The deactivation constant  $k_d$  had similar values for all three cycles,  $\sim 0.87-1.65 \text{ h}^{-1}$ , which corresponds to the mean life values of ~0.6-1.15 h. According to Table 2, each new cycle started with a slightly greater initial propylene consumption rate,  $r_0$  of the first cycle > second cycle > third cycle, however, the predicted steady-state rates only marginally increased with each regeneration. The mean life of the third cycle was shorter than that of the first and second cycles because the initial rate of the third cycle was the highest and it reached almost identical steady-state rate as the first and second cycles,

Table 3 Distribution of products formed on Ni-POM-WD/SBA-15 over different cycles at under steady-state conditions at 180 °C and 1.01 bar

| Product                          | Steady-state<br>selectivity<br>during cycle<br>1 (%) | Steady-state<br>selectivity<br>during cycle<br>2 (%) | Steady-state<br>selectivity<br>during cycle<br>3 (%) |
|----------------------------------|--|--|--|
| 1-Hexene                         | 3.7  | 3.9  | 4.0  |
| cis-2-Hexene                     | 14.2   | 14.0   | 14.1   |
| cis-3-Hexene                     | 12.0   | 11.7   | 11.4   |
| trans-2-Hexene                   | 32.7   | 32.3   | 32.5   |
| trans-3-Hexene                   | 18.6   | 18.7   | 19.0   |
| 4-Methyl-1-pentene               | 4.7  | 4.7  | 4.7  |
| 2-Methyl-2-pentene               | 1.1  | 1.3  | 1.3  |
| <i>trans</i> -4-Methyl-2-pentene | 12.0   | 12.3   | 12.0   |
| 2,3-Dimethyl-1-butene            | 1.0  | 1.1  | 1.0  |
| Conversion (%)                   | 0.23   | 0.22   | 0.25   |

resulting in a somewhat greater  $k_d$ . The enhancement in the initial rates could be due to the improved dispersion/redispersion of the Ni-POM-WD particles occurring from the elevated temperature of the regeneration process. Moreover, the product distribution for three reaction-regeneration cycles at steady-state conversions and averaged conversions after 300 min of TOS are summarized in Table 3. The regeneration process did not affect the product distribution, remaining 100% selective towards dimer products with preference for the linear dimers at around ~80% selectivity. This indicates that the active sites remain unaltered throughout the reaction and regeneration process.

HAADF-STEM imaging and Ni EDX mapping of Ni-POM-WD/SBA-15 post propylene oligomerization is shown in Fig. 7. Elemental maps of P, K, W, O, and Si are given in Fig. S6.† The HAADF-STEM images show that the Ni-POM-WD particles are well distributed throughout the pores of the SBA-15 support. Ni EDX mapping shows that the Ni is well dispersed after reaction, showing no signs of agglomeration. The solid-state MAS <sup>31</sup>P NMR of Ni-POM-WD/SBA-15 after the propylene oligomerization reaction is similar to that of the fresh catalyst (Fig. S5b†), indicating no signs of the POM-WD structure changing or Ni sites leaving the POMs. The fact that the Ni-POM-WD can be fully regenerated using a high temperature helium treatment and the lack of modification of the material observed with HAADF-STEM imaging, EDX mapping, and MAS <sup>31</sup>P NMR indicates that the observed deactivation of the Ni<sup>2+</sup> sites is reversible, and the Ni-POM-WD clusters perhaps redisperse during the regeneration treatment.

Table 2 Best fit parameters  $(r_0, r_{ss}, k_d)$  for propylene consumption rate on Ni-POM-WD/SBA-15 using a second-order deactivation model

| Cycle  | $r_0$ at $t = 0^b$ (mol C <sub>3</sub> /mol Ni per h) | ${r_{\rm ss}}^c$ (mol C <sub>3</sub> /mol Ni per h) | $k_{\mathrm{d}}^{d}\left(\mathrm{h}^{-1}\right)$ | Mean life $1/k_d^e$ (h) |
|--------|---|---|--|-------------------------|
| First  | 8.20  | 0.89  | 1.12   | 0.85                    |
| Second | 8.83  | 0.96  | 0.87   | 1.15                    |
| Third  | 11.10   | 1.50  | 1.65   | 0.61                    |

<sup>&</sup>lt;sup>a</sup> Second-order deactivation model:  $r(t) = \frac{r_{\rm i}}{1+k_{\rm d}t} + r_{\rm ss}$ . <sup>b</sup>  $r_{\rm 0} = r_{\rm i} + r_{\rm ss}$ . <sup>c</sup>  $r_{\rm ss}$  steady-state rate. <sup>d</sup>  $k_{\rm d}$  deactivation constant. <sup>e</sup> Reciprocal of the deactivation constant.

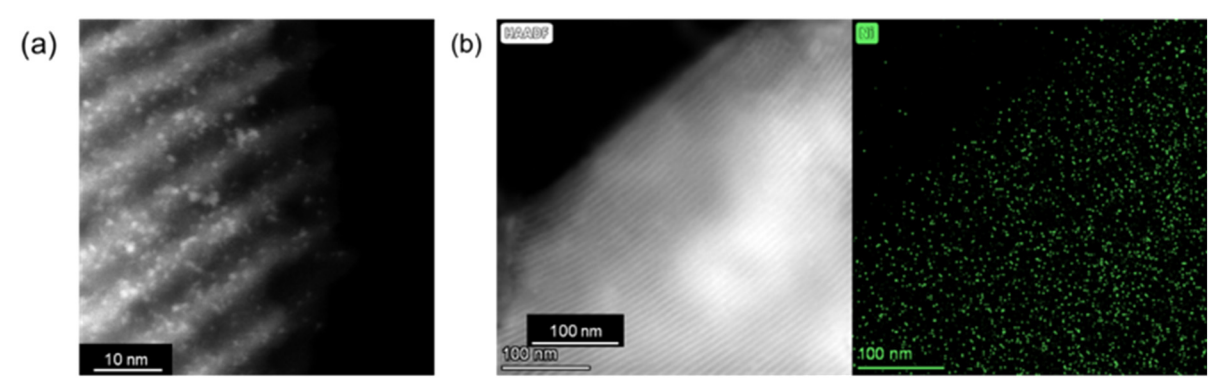


Fig. 7 (a) HAADF-STEM image and (b) EDX Ni mapping of Ni-POM-WD/SBA-15 post propylene oligomerization at 180 °C and 1 bar.

# 4. Conclusion

Here, we report the catalytic performance of isolated Ni<sup>2+</sup> sites in Ni-POM-WD/SBA-15 for propylene oligomerization and the resulting product distribution. Remarkably, Ni-POM-WD/SBA-15 was highly selective (>76%) to linear dimerization products with 100% selectivity to C6 products. The deactivated Ni-POM-WD/SBA-15 was also found to be regenerable after propylene oligomerization using hightemperature helium treatment. This is consistent with previously reported ethylene oligomerization results with this material.<sup>59</sup> These results demonstrate the versatility of isolated Ni active sites in POMs, and highlights the stability and recyclability of these materials as heterogeneous catalysts for the production of linear alkenes from a variety of olefins without addition of a co-catalyst. The modification of lacunary defects in POMs could serve as a platform for isolating Ni for other reactions, such as 1-butene oligomerization or for isolating other metal cations, thus opening the door for a wider range of catalytic applications.

# Conflicts of interest

There are no conflicts to declare.

# Acknowledgements

This work was supported primarily by the Engineering Research Centers Program of the National Science Foundation under NSF Cooperative Agreement no. EEC-1647722. The authors would also like to thank the Notre Dame Integrated Imaging Facility, the Notre Dame Molecular Structure Facility, the Notre Dame Magnetic Resonance Research Center, and the Notre Dame Centre for Environmental Science and Technology for use of their facilities.

# Notes and references

- 1 H. Olivier-Bourbigou, P. A. R. Breuil, L. Magna, T. Michel, M. F. Espada Pastor and D. Delcroix, Chem. Rev., 2020, 120, 7919–7983.
- 2 S. Vernuccio, E. E. Bickel, R. Gounder and L. J. Broadbelt, ACS Catal., 2019, 9, 8996-9008.

- 3 A. Corma and S. Iborra, in Catalysts for Fine Chemical Synthesis, ed. E. G. Derouane, John Wiley & Sons Ltd., West Sussex, 2006, vol. 4, pp. 125-140.
- 4 A. Bollmann, K. Blann, J. T. Dixon, F. M. Hess, E. Killian, H. Maumela, D. S. McGuinness, D. H. Morgan, A. Neveling, S. Otto, M. Overett, A. M. Z. Slawin, P. Wasserscheid and S. Kuhlmann, J. Am. Chem. Soc., 2004, 126, 14712-14713.
- 5 C. T. O'Connor and M. Kojima, Catal. Today, 1990, 6, 329-349.
- 6 V. C. Gibson, C. Redshaw and G. A. Solan, Chem. Rev., 2007, 107, 1745-1776.
- 7 B. L. Small and A. J. Marcucci, Organometallics, 2001, 20, 5738-5744.
- 8 K. P. Tellmann, V. C. Gibson, A. J. P. White and D. J. Williams, Organometallics, 2005, 24, 280-286.
- 9 C. Bianchini, G. Giambastiani, I. G. Rios, A. Meli, A. M. Segarra, A. Toti and F. Vizza, J. Mol. Catal. A: Chem., 2007, 277, 40-46.
- 10 A. Behr, N. Rentmeister, T. Seidensticker, T. A. Faßbach, S. Peitz and D. Maschmeyer, J. Mol. Catal. A: Chem., 2014, 395, 355-363.
- 11 D. L. Beach, J. E. Bozik, C. Y. Wu and Y. V. Kissin, J. Mol. Catal., 1986, 34, 345-354.
- 12 B. Lian, K. Beckerle, T. P. Spaniol and J. Okuda, Angew. Chem., Int. Ed., 2007, 46, 8507-8510.
- 13 J. Skupińska, Chem. Rev., 1991, 91, 613-648.
- 14 D. Vogt, in Applied homogeneous catalysis with organometallic compounds: a comprehensive handbook, ed. B. Cornils and W. A. Herrmann, Wiley-VCH Verlag, Weinheim, 2nd edn, 2002, vol. 1, pp. 240-253.
- 15 L. Bonneviot, D. Olivier and M. Che, J. Mol. Catal., 1983, 21,
- 16 F. X. Cai, C. Lepetit, M. Kermarec and D. Olivier, J. Mol. Catal., 1987, 43, 93-116.
- 17 J. Heveling, C. P. Nicolaides and M. S. Scurrell, J. Chem. Soc., Chem. Commun., 1991, 126-127.
- 18 M. Lallemand, A. Finiels, F. Fajula and V. Hulea, J. Phys. Chem. C, 2009, 113, 20360-20364.
- 19 P.-A. R. Breuil, L. Magna and H. Olivier-Bourbigou, Catal. Lett., 2015, 145, 173-192.

- 20 C. Bianchini, G. Giambastiani, L. Luconi and A. Meli, Coord. Chem. Rev., 2010, 254, 431-455.
- 21 M. A. Deimund, J. Labinger and M. E. Davis, ACS Catal., 2014, 4, 4189-4195.
- 22 A. N. Mlinar, O. C. Ho, G. G. Bong and A. T. Bell, ChemCatChem, 2013, 5, 3139-3147.
- 23 X. Li, D. Han, H. Wang, G. Liu, B. Wang, Z. Li and J. Wu, Fuel, 2015, 144, 9-14.
- 24 A. Finiels, F. Fajula and V. Hulea, Catal. Sci. Technol., 2014, 4, 2412-2426.
- 25 R. Joshi, A. Saxena and R. Gounder, Catal. Sci. Technol., 2020, 10, 7101-7123.
- 26 V. Hulea and F. Fajula, J. Catal., 2004, 225, 213-222.
- 27 A. N. Mlinar, G. B. Baur, G. G. Bong, A. B. Getsoian and A. T. Bell, J. Catal., 2012, 296, 156-164.
- 28 A. Saxena, R. Joshi, R. R. Seemakurthi, E. Koninckx, L. J. Broadbelt, J. Greeley and R. Gounder, ACS Eng. Au, 2022, 2, 12-16.
- 29 A. N. Mlinar, B. K. Keitz, D. Gygi, E. D. Bloch, J. R. Long and A. T. Bell, ACS Catal., 2014, 4, 717-721.
- 30 R. J. Comito, E. D. Metzger, Z. Wu, G. Zhang, C. H. Hendon, J. T. Miller and M. Dincă, Organometallics, 2017, 36, 1681-1683.
- 31 U. S. F. Arrozi, V. Bon, C. Kutzscher, I. Senkovska and S. Kaskel, Dalton Trans., 2019, 48, 3415-3421.
- 32 K. Kyogoku, C. Yamada, Y. Suzuki, S. Nishiyama, K. Fukumoto, H. Yamamoto, S. Indo, M. Sano and T. Miyake, J. Jpn. Pet. Inst., 2010, 53, 308-312.
- 33 J. Canivet, S. Aguado, Y. Schuurman and D. Farrusseng, J. Am. Chem. Soc., 2013, 135, 4195-4198.
- 34 I. V. Kozhevnikov, Chem. Rev., 1998, 98, 171-198.
- 35 T. Okuhara, N. Mizuno and M. Misono, Adv. Catal., 1996, 41, 113-252.
- 36 M. T. Pope and A. Muller, Polyoxometalates: From Platonic Solids to Anti-Retroviral Activity, Kluwer Academic Publishers, Dordrecht, The Netherlands, 1994.
- 37 J. Tang, X. L. Yang, X. W. Zhang, M. Wang and C. de Wu, Dalton Trans., 2010, 39, 3396-3399.
- 38 L. X. Shi, X. W. Zhang and C. de Wu, Dalton Trans., 2011, 40, 779-781.
- 39 N. Mizuno, K. Yamaguchi and K. Kamata, in Coordination Chemistry Reviews, 2005, vol. 249, pp. 1944-1956.
- 40 M. Misono, Catal. Rev.: Sci. Eng., 1987, 29, 269-321.
- 41 F. Lefebvre, F. X. Liu-Cai and A. Auroux, J. Mater. Chem., 1994, 4, 125-131.
- 42 C. Y. Sun, S. X. Liu, D. D. Liang, K. Z. Shao, Y. H. Ren and Z. M. Su, J. Am. Chem. Soc., 2009, 131, 1883-1888.
- 43 I. V. Kozhevnikov, Catal. Rev.: Sci. Eng., 1995, 37, 311-352.
- 44 M. L. Sarazen, E. Doskocil and E. Iglesia, J. Catal., 2016, 344, 553-569.
- 45 M. N. Timofeeva, Appl. Catal., A, 2003, 256, 19–35.
- 46 J. Macht, M. J. Janik, M. Neurock and E. Iglesia, Angew. Chem., Int. Ed., 2007, 46, 7864-7868.
- 47 L. C. W. Baker and D. C. Glick, Chem. Rev., 1998, 98, 3-50.
- 48 Q. W. Song, B. Yu, X. D. Li, R. Ma, Z. F. Diao, R. G. Li, W. Li and L. N. He, Green Chem., 2014, 16, 6700-6703.

- 49 K. Sugahara, T. Kimura, K. Kamata, K. Yamaguchi and N. Mizuno, Chem. Commun., 2012, 48, 8422-8424.
- 50 S. Itagaki, K. Kamata, K. Yamaguchi and N. Mizuno, ChemCatChem, 2013, 5, 1725-1728.
- 51 A. Yoshida, S. Hikichi and N. Mizuno, J. Organomet. Chem., 2007, 692, 455-459.
- 52 S. Zhao, Y. Chen and Y. F. Song, Appl. Catal., A, 2014, 475, 140-146.
- 53 A. Patel and N. Narkhede, Catal. Sci. Technol., 2013, 3, 3317-3325.
- 54 K. T. Venkateswara Rao, P. S. Sai Prasad and N. Lingaiah, I. Mol. Catal. A: Chem., 2009, 312, 65-69.
- 55 J. S. Yadav, B. V. Subba Reddy, K. V. Purnima, S. Jhansi, K. Nagaiah and N. Lingaiah, Catal. Commun., 2008, 9, 2361-2364.
- 56 J. S. Yadav, B. V. S. Reddy, S. Praveenkumar, K. Nagaiah, N. Lingaiah and P. S. Saiprasad, Synthesis, 2004, 901–904.
- 57 J. H. Choi, J. K. Kim, D. R. Park, T. H. Kang, J. H. Song and I. K. Song, J. Mol. Catal. A: Chem., 2013, 371, 111-117.
- 58 J. H. Choi, J. K. Kim, S. Park, J. H. Song and I. K. Song, Appl. Catal., A, 2012, 427-428, 79-84.
- 59 Y. Cho, J. A. Muhlenkamp, A. G. Oliver and J. C. Hicks, Chem. Commun., 2021, 57, 13772-13775.
- 60 K. Toch, J. W. Thybaut and G. B. Marin, Appl. Catal., A, 2015, 489, 292-304.
- 61 K. Toch, J. W. Thybaut, M. A. Arribas, A. Martínez and G. B. Marin, Chem. Eng. Sci., 2017, 173, 49-59.
- 62 G. V. S. Seufitelli and R. Gustafson, Ind. Eng. Chem. Res., 2022, 61, 4286-4299.
- 63 D. K. Lyon, W. K. Miller, T. Novet, P. J. Domaille, E. Evitt, D. C. Johnson and R. G. Finke, J. Am. Chem. Soc., 1991, 113, 7209-7221.
- 64 B. J. Hornstein and R. G. Finke, Inorg. Chem., 2002, 41, 2720-2730.
- 65 J. C. Hicks and C. W. Jones, Langmuir, 2006, 22, 2676-2681.
- 66 D. Zhao, J. Feng, Q. Huo, N. Melosh, G. H. Fredrickson, B. F. Chmelka and G. D. Stucky, Science, 1979, 1998(279), 548-552.
- 67 Z. Xu, J. P. Chada, L. Xu, D. Zhao, D. C. Rosenfeld, J. L. Rogers, I. Hermans, M. Mavrikakis and G. W. Huber, ACS Catal., 2018, 8, 2488-2497.
- 68 Z. Xu, J. P. Chada, D. Zhao, C. A. Carrero, Y. T. Kim, D. C. Rosenfeld, J. L. Rogers, S. J. Rozeveld, I. Hermans and G. W. Huber, ACS Catal., 2016, 6, 3815-3825.
- 69 R. Joshi, G. Zhang, T. Miller and R. Gounder, ACS Catal., 2018, 8, 11407-11422.
- 70 A. Forestière, H. Olivier-Bourbigou and L. Saussine, Oil Gas Sci. Technol., 2009, 64, 649-667.
- 71 R. Y. Brogaard and U. Olsbye, ACS Catal., 2016, 6, 1205-1214.
- 72 I. Agirrezabal-Telleria and E. Iglesia, J. Catal., 2020, 389, 690-705.
- 73 Y. M. Liu and B. Smit, ACS Catal., 2017, 7, 3940-3948.
- 74 A. Ehrmaier, Y. Liu, S. Peitz, A. Jentys, Y.-H. C. Chin, M. Sanchez-Sanchez, R. Bermejo-Deval and J. Lercher, ACS Catal., 2019, 9, 315-324.

- 75 R. Caulkins, R. Joshi, R. Gounder and F. H. Ribeiro, *ChemCatChem*, 2022, **14**(1), e202101478.
- 76 R. Y. Brogaard, M. Kømurcu, M. M. Dyballa, A. Botan, V. van Speybroeck, U. Olsbye and K. de Wispelaere, ACS Catal., 2019, 9, 5645–5650.
- 77 G. V. S. Seufitelli, J. J. W. Park, P. N. Tran, A. Dichiara, F. L. P. Resende and R. Gustafson, *J. Catal.*, 2021, **401**, 40–53.
- 78 G. Egloff and E. Wilson, *Ind. Eng. Chem.*, 1935, 27, 917–933.
- 79 G. Egloff and C. I. Parrish, Chem. Rev., 1936, 19, 145-161.
- 80 G. Egloff, Ind. Eng. Chem., 1936, 28, 1461-1467.
- 81 J. B. Butt and E. E. Petersen, *Activation, deactivation, and poisoning of catalysts*, Academic Press, Inc., San Diego, 1988.